

## A Time Splitting Space Spectral Element Method for the Cahn-Hilliard Equation

Lizhen Chen<sup>1</sup> and Chuanju Xu<sup>2,\*</sup>

<sup>1</sup> Beijing Computational Science Research Center, Beijing 100084, China.

<sup>2</sup> School of Mathematical Sciences, Xiamen University, Xiamen 361005, China.

Received 15 July 2013; Accepted (in revised version) 18 November 2013

Available online 28 November 2013

---

**Abstract.** We propose and analyse a class of fully discrete schemes for the Cahn-Hilliard equation with Neumann boundary conditions. The schemes combine large-time step splitting methods in time and spectral element methods in space. We are particularly interested in analysing a class of methods that split the original Cahn-Hilliard equation into lower order equations. These lower order equations are simpler and less computationally expensive to treat. For the first-order splitting scheme, the stability and convergence properties are investigated based on an energy method. It is proven that both semi-discrete and fully discrete solutions satisfy the energy dissipation and mass conservation properties hidden in the associated continuous problem. A rigorous error estimate, together with numerical confirmation, is provided. Although not yet rigorously proven, higher-order schemes are also constructed and tested by a series of numerical examples. Finally, the proposed schemes are applied to the phase field simulation in a complex domain, and some interesting simulation results are obtained.

**AMS subject classifications:** 65M06, 65M12, 65N30, 65N35, 76A05

**Key words:** Cahn-Hilliard, time splitting schemes, spectral methods, error analysis.

---

### 1. Introduction

The Cahn-Hilliard equation, originally introduced by Cahn and Hilliard to describe the phase separation and coarsening phenomena in a melted alloy [3], has now been used to model many moving interface problems from fluid dynamics to materials science via a phase-field approach — e.g. see Refs. [4, 5, 9, 21, 23, 25, 26, 28, 31]. Usually, the Cahn-Hilliard equation takes the form

$$\partial_t u + \Delta \left( \Delta u - \frac{1}{\varepsilon^2} f(u) \right) = 0, \quad 0 < t \leq T, \mathbf{x} \in \Omega, \quad (1.1)$$

---

\*Corresponding author. Email addresses: lzchen@csrcc.ac.cn (L. Chen), cjxu@xmu.edu.cn (C. Xu)

where  $\Omega \subset \mathbb{R}^d$  (for  $d = 2, 3$ ) is a bounded domain,  $f(u) = F'(u)$  with  $F(u)$  a given energy potential, the parameter  $\varepsilon$  denotes the interfacial width that is small compared to the characteristic length of the problem under consideration, and  $\Delta$  denotes the Laplacian operator. This fourth-order equation can be viewed as the gradient flow of the Liapunov energy functional

$$E(u) = \int_{\Omega} \left[ \frac{1}{2} |\nabla u|^2 + \frac{1}{\varepsilon^2} F(u) \right] d\mathbf{x} \quad (1.2)$$

in the space  $H^{-1}(\Omega)$ .

Another commonly used model in the investigation of moving surface problems is the Allen-Cahn equation (e.g. see Refs. [1, 10, 11, 19, 22]):

$$\partial_t u - \Delta u + \frac{1}{\varepsilon^2} f(u) = 0, \quad (1.3)$$

which was first introduced by Allen and Cahn [1] to describe the motion of antiphase boundaries in crystalline solids. Similar to the Cahn-Hilliard equation, Eq. (1.3) can be viewed as the gradient flow of the same Liapunov energy functional  $E(u)$  defined in Eq. (1.2) in the space  $L^2(\Omega)$ . Both equations (1.1) and (1.3) satisfy the energy law

$$\partial_t E(u(t)) \leq 0,$$

but each of them has its own advantages. Roughly speaking, the Allen-Cahn equation satisfies the maximum principle, and the computation is cheaper since it is a second-order equation. By contrast, the Cahn-Hilliard equation does not satisfy the maximum principle, but possesses conservation of total mass for the system, which is very important for some practical applications — e.g. the mixture of two incompressible fluids [23] or liquid crystal flows [24, 27].

Numerical methods for the Cahn-Hilliard equation can be found in many references — cf. [6–8, 12–18, 20, 30, 32, 33] and other references therein. Existing numerical techniques include finite element schemes [7, 13, 15, 16, 20], finite difference approaches [2, 17], and combined spectral and large-time stepping methods [33]. Compared to a standard conforming finite element method, which requires that the approximation space is a subspace of  $H^2$ , the methods based on a splitting technique [7, 18, 29, 32] only require  $C^0$ -continuity of the approximate solution and are therefore easier to implement. In this article, we analyse an approach for the Cahn-Hilliard equation using splitting schemes in time and spectral element methods in space. Our main purpose is to establish the stability and convergence properties of the proposed scheme, together with an extension to the spectral element method for the spatial discretisation. We are aware that similar analysis has been carried out in Refs. [18, 32], where an error estimate was obtained assuming boundedness of the discrete solution, but that assumption is only valid in the one-dimensional case for the standard energy potential. To overcome this difficulty, we consider here the two-dimensional Cahn-Hilliard equation corresponding to a truncated potential  $F(u)$  with quadratic growth

at infinities [6, 13], such that boundedness of the solution can be obtained [4]. To further improve the stability, we propose to add an extra stability term as in Ref. [29]. More precisely, we consider the initial-boundary-value problem for the Cahn-Hilliard equation

$$\partial_t u + \Delta \left( \Delta u - \frac{1}{\varepsilon^2} f(u) \right) = 0, \quad (\mathbf{x}, t) \in \Omega \times (0, T), \tag{1.4}$$

$$\frac{\partial u}{\partial \mathbf{n}} = \frac{\partial^3 u}{\partial n^3} = 0, \quad \mathbf{x} \in \partial\Omega, \quad 0 < t < T, \tag{1.5}$$

$$u(\mathbf{x}, 0) = u_0(\mathbf{x}), \quad \mathbf{x} \in \Omega, \tag{1.6}$$

where  $\Omega = (0, L_1) \times (0, L_2)$ ,  $u_0$  is a given initial function,  $\mathbf{n}$  is the outward normal to  $\partial\Omega$ , and  $F(u)$  is the truncated double-well potential defined by

$$F(u) = \begin{cases} \frac{1}{2}(u - 1)^2, & u > 1, \\ \frac{1}{4}(u^2 - 1)^2, & |u| \leq 1, \\ -\frac{1}{2}(u - 1)^2, & u < -1, \end{cases}$$

such that

$$f(u) = F'(u) = \begin{cases} u - 1, & u > 1, \\ u^3 - u, & |u| \leq 1, \\ -(u - 1), & u < -1. \end{cases}$$

It is an easy matter to verify that

$$\|f(u)\|_0 \leq \|u\|_0, \quad |f'(u)| \leq 1 \quad \text{and} \quad |f(u_1) - f(u_2)| \leq |u_1 - u_2|. \tag{1.7}$$

This article is organised as follows. We discuss a semi-discrete approximation of the Cahn-Hilliard equation in Section 2, and prove the existence and uniqueness of the semi-discrete solution. In Section 3, the fully discrete approximation is constructed, and its stability and convergence properties are investigated. In particular, the consequence of the extra stability term for the error is made evident. We present some numerical results in Section 4, which validate the error estimates and confirm that larger time-steps can be used by adding a consistent extra term. Some simulations of two incompressible fluids using our proposed method are also discussed in Section 4, followed by concluding remarks in Section 5.

## 2. Semi-Discrete Problem: A Spectral Element Method in Space

We start by introducing an auxiliary function  $w =: (1/\varepsilon^2)f(u) - \Delta u$ , and reformulating Eqs. (1.4)–(1.6) as follows:

$$u_t - \Delta w = 0, \quad \mathbf{x} \in \Omega, \quad 0 < t \leq T, \quad (2.1)$$

$$-\Delta u + \frac{1}{\varepsilon^2}f(u) - w = 0, \quad \mathbf{x} \in \Omega, \quad 0 < t \leq T, \quad (2.2)$$

$$\frac{\partial u}{\partial \mathbf{n}} = \frac{\partial w}{\partial \mathbf{n}} = 0, \quad \mathbf{x} \in \partial\Omega, \quad 0 < t \leq T, \quad (2.3)$$

$$u(\mathbf{x}, 0) = u_0(\mathbf{x}), \quad \mathbf{x} \in \Omega. \quad (2.4)$$

The variational formulation of problem (2.1)–(2.4) is as follows. Given  $u_0 \in H^1(\Omega)$  and  $\forall t \in (0, T]$ , find  $u(t) \in H^1(\Omega)$  and  $w(t) \in H^1(\Omega)$  such that

$$\partial_t(u(t), v) + (\nabla w(t), \nabla v) = 0, \quad \forall v \in H^1(\Omega), \quad (2.5)$$

$$(\nabla u(t), \nabla \chi) + \left( \frac{1}{\varepsilon^2}f(u(t)) - w(t), \chi \right) = 0, \quad \forall \chi \in H^1(\Omega), \quad (2.6)$$

$$u(\mathbf{x}, 0) = u_0(\mathbf{x}), \quad \mathbf{x} \in \Omega. \quad (2.7)$$

In the consequent space discretisation of the problem (2.5)–(2.7), the spectral element aspect proceeds by breaking the domain  $\Omega$  into a number of non-overlapping elements

$$\bar{\Omega} = \bigcup_{k=1}^K \bar{\Omega}_k, \quad \Omega_k \cap \Omega_l = \emptyset, \quad k \neq l,$$

and to simplify our analysis we assume all elements are rectilinear. In particular, we let  $h = \max\{h_i^k, i = 1, 2; k = 1, \dots, K\}$ , where  $h_1^k$  and  $h_2^k$  are the lengths of the rectangle  $\Omega_k$  in the two directions, respectively.

Hereafter we use  $\mathbf{N}$  to denote the parameter pair  $(N, K)$ , when the piecewise polynomials space is defined as follows:

$$P_{\mathbf{N}}(\Omega) = \{\phi \in L^2(\Omega); \phi|_{\Omega_k} \in P_N(\Omega_k), 1 \leq k \leq K\},$$

where  $P_N(\Omega_k)$  denotes the space of all polynomials of degree  $\leq N$  with respect to each variable in  $\Omega_k$ . In particular, if  $K = 1$ , we denote  $P_{\mathbf{N}}(\Omega)$  by  $P_N(\Omega)$ . In what follows,  $c$  means a generic constant, which may depend on the solution  $u$  but is independent of the discretisation parameters.

The spectral element approximation to the problem (2.5)–(2.7) thus reads as follows. For all  $t \in (0, T]$ , find  $u_{\mathbf{N}}(t) \in P_{\mathbf{N}}(\Omega)$ ,  $w_{\mathbf{N}}(t) \in P_{\mathbf{N}}(\Omega)$  such that

$$\partial_t(u_{\mathbf{N}}(t), v_{\mathbf{N}}) + (\nabla w_{\mathbf{N}}(t), \nabla v_{\mathbf{N}}) = 0, \quad \forall v_{\mathbf{N}} \in P_{\mathbf{N}}(\Omega), \quad (2.8)$$

$$(\nabla u_{\mathbf{N}}(t), \nabla \chi_{\mathbf{N}}) + \left( \frac{1}{\varepsilon^2}f(u_{\mathbf{N}}(t)) - w_{\mathbf{N}}(t), \chi_{\mathbf{N}} \right) = 0, \quad \forall \chi_{\mathbf{N}} \in P_{\mathbf{N}}(\Omega), \quad (2.9)$$

$$u_{\mathbf{N}}(0) = u_{0,\mathbf{N}}, \quad (2.10)$$

where  $u_{0,\mathbf{N}}$  is an approximation of  $u_0$ .

**Lemma 2.1.** *If  $u_{0,N} \in H^1(\Omega)$  and  $(u_N, w_N)$  is a solution of Eqs. (2.8)–(2.10), then*

$$\partial_t E(u_N(t)) + \|\nabla w_N(t)\|_0^2 = 0. \tag{2.11}$$

*Proof.* It can be verified directly that

$$\begin{aligned} \partial_t E(u_N) &= \int_{\Omega} \left[ \nabla u_N(t) \cdot \partial_t \nabla u_N(t) + \frac{1}{\varepsilon^2} f(u_N(t)) \partial_t u_N(t) \right] dx \\ &\stackrel{\text{by (2.9)}}{=} (w_N(t), \partial_t u_N(t)) \\ &\stackrel{\text{by (2.8)}}{=} -\|\nabla w_N(t)\|_0^2, \end{aligned}$$

leading to Eq. (2.11). □

**Lemma 2.2.**  $(u_N(t), 1) = (u_{0,N}, 1), \forall t > 0.$

*Proof.* This follows from Eq. (2.8) by setting  $v_N = 1$ . □

**Lemma 2.3.** *If  $u_{0,N}, u_0 \in H^1(\Omega)$ ,  $\|u_{0,N}\|_1 \leq c_0 \|u_0\|_1$  and  $(u_{0,N}, 1) = (u_0, 1)$ , then there exists a constant  $c(u_0)$  such that*

$$\|u_N(t)\|_1 \leq c(u_0), \quad \forall t \in (0, T). \tag{2.12}$$

*Proof.* From Lemma 2.1,  $E(u_N) \leq E(u_{0,N})$  — i.e.

$$\frac{1}{2} |u_N|_1^2 + \frac{1}{\varepsilon^2} \int_{\Omega} F(u_N(t)) dx \leq \frac{1}{2} |u_{0,N}|_1^2 + \frac{1}{\varepsilon^2} \int_{\Omega} F(u_{0,N}(t)) dx.$$

It is known from the Young inequality that there exist two constants  $c_1$  and  $c_2$  such that

$$\frac{1}{8} u^4 - c_1 \leq F(u) \leq \frac{1}{2} u^4 + c_2.$$

Together with the embedding theorem  $H^1(\Omega) \hookrightarrow L^4(\Omega)$ , this gives

$$\begin{aligned} \frac{1}{2} |u_N|_1^2 + \frac{1}{8\varepsilon^2} \int_{\Omega} u_N^4(t) dx &\leq c_3 + \frac{1}{2} |u_{0,N}|_1^2 + \frac{1}{2\varepsilon^2} \int_{\Omega} u_{0,N}^4(t) dx \\ &\leq c_3 + \frac{1}{2} |u_{0,N}|_1^2 + \frac{c}{2\varepsilon^2} \|u_{0,N}\|_1^4 \\ &\leq c_3 + c_4 \|u_0\|_1^2 + c_5 \|u_0\|_1^4. \end{aligned}$$

Furthermore, from the Poincaré inequality and Lemma 2.2 we obtain

$$\begin{aligned} \|u_N(t)\|_1 &\lesssim |u_N(t)|_1 + |(u_N(t), 1)| \\ &\lesssim |u_N(t)|_1 + |(u_{0,N}, 1)| \\ &\lesssim c_3 + c_4 \|u_0\|_1^2 + c_5 \|u_0\|_1^4 + |(u_0, 1)| \\ &:= c(u_0). \end{aligned}$$

This completes the proof. □

**Theorem 2.1.** *Under the same assumptions as in Lemma 2.3, the semi-discrete problem (2.8)–(2.10) admits a unique solution  $(u_N, w_N) \in L^\infty[(0, T), H^1(\Omega)] \times L^2[(0, T), H^1(\Omega)]$ .*

*Proof.* Subtracting Eq. (2.8) with  $v_N = u_N(t)$  from Eq. (2.9) with  $\chi_N = w_N(t)$  gives

$$\begin{aligned} \frac{1}{2} \partial_t \|u_N(t)\|_0^2 + \|w_N(t)\|_0^2 &= \frac{1}{\varepsilon^2} (f(u_N(t)), w_N(t)) \\ &\leq \frac{1}{2\varepsilon^4} \|f(u_N(t))\|_0^2 + \frac{1}{2} \|w_N(t)\|_0^2, \end{aligned}$$

hence from (1.7) we get

$$\partial_t \|u_N(t)\|_0^2 + \|w_N(t)\|_0^2 \leq \frac{1}{\varepsilon^4} \|u_N(t)\|_0^2.$$

Applying the Gronwall inequality then yields

$$\|u_N(t)\|_0^2 \leq \|u_{0,N}\|_0^2 e^{T/\varepsilon^4} \leq \|u_{0,N}\|_1^2 e^{T/\varepsilon^4} \lesssim \|u_0\|_1^2 e^{T/\varepsilon^4}, \quad 0 \leq t \leq T, \quad (2.13)$$

$$\int_0^t \|w_N(\tau)\|_0^2 d\tau \lesssim T \|u_0\|_1^2 e^{T/\varepsilon^4}, \quad 0 \leq t \leq T. \quad (2.14)$$

From Eq. (2.11) we obtain

$$\begin{aligned} \int_0^t \|w_N(\tau)\|_1^2 d\tau &= -\frac{1}{2} \int_0^t \partial_t \|\nabla u_N(t)\|_0^2 dt - \frac{1}{\varepsilon^2} \int_\Omega \int_0^t \partial_t F(u_N(t)) dt dx \\ &= -\frac{1}{2} (\|\nabla u_N(t)\|_0^2 - \|\nabla u_N(0)\|_0^2) - \frac{1}{\varepsilon^2} \int_\Omega (F(u_N(t)) - F(u_N(0))) dx \\ &\lesssim c(u_0), \end{aligned} \quad (2.15)$$

where we have used the fact that  $|\int_\Omega (F(u_N(t)) dx)| \leq \|u_N(t)\|_4^4 + c \leq \|u_N(t)\|_1^4 + c$ . Combining Eqs. (2.13) and (2.15) gives

$$\int_0^t \|w_N(\tau)\|_1^2 d\tau \lesssim c(u_0), \quad \forall t \in (0, T]. \quad (2.16)$$

Finally, we obtain the desired result from inequalities (2.12) and (2.16). □

Now we carry out an error analysis for the semi-discrete solution. To this end, we introduce some notation.

The operator  $\Pi_N : H^1(\Omega) \rightarrow P_N(\Omega)$  is defined as follows. For all  $v \in H^1(\Omega)$  we have  $\Pi_N v \in P_N(\Omega)$  where

$$\begin{aligned} (\nabla(\Pi_N v - v), \nabla \chi) &= 0, \quad \forall \chi \in P_N(\Omega) \text{ such that } (\chi, 1) = 0, \\ (\Pi_N v - v, 1) &= 0. \end{aligned}$$

Note that from the first condition we can easily check that

$$(\nabla(\Pi_N v - v), \nabla \chi) = 0, \quad \forall \chi \in P_N(\Omega). \quad (2.17)$$

The following approximation result is well known — e.g. see [34].

**Lemma 2.4.** For any  $u \in H^m(\Omega)$  with  $m \geq 1$ ,

$$\|u - \Pi_{\mathbf{N}}u\|_0 \leq ch^{\min(N+1,m)}N^{-m}\|u\|_m,$$

where  $c$  is a constant independent of  $\mathbf{N}$  and  $u$ .

**Theorem 2.2.** If  $u_0 \in H^1(\Omega)$ ,  $u_{0,\mathbf{N}} = \Pi_{\mathbf{N}}u_0$  and the solution  $(u, w)$  of (2.5)–(2.7) satisfies  $u, \partial_t u \in L^\infty((0, T), H^m(\Omega))$  and  $w \in L^2((0, T), H^m(\Omega))$ , then the solution  $(u_{\mathbf{N}}, w_{\mathbf{N}})$  of (2.8)–(2.10) satisfies the following error estimate:

$$\|u - u_{\mathbf{N}}\|_{L^\infty((0,T),L^2(\Omega))} + \|w - w_{\mathbf{N}}\|_{L^2((0,T),L^2(\Omega))} \lesssim h^{\min(N+1,m)}N^{-m}. \quad (2.18)$$

*Proof.* Let

$$E_{\mathbf{N}}(t) = u_{\mathbf{N}}(t) - \Pi_{\mathbf{N}}u(t), \quad e_{\mathbf{N}}(t) = w_{\mathbf{N}}(t) - \Pi_{\mathbf{N}}w(t).$$

Then from Eq. (2.17), for all  $v_{\mathbf{N}} \in P_{\mathbf{N}}(\Omega)$ ,  $\chi_{\mathbf{N}} \in P_{\mathbf{N}}(\Omega)$  and for all  $t \in (0, T]$  we have

$$\begin{aligned} (\partial_t E_{\mathbf{N}}(t), v_{\mathbf{N}}) + (\nabla e_{\mathbf{N}}(t), \nabla v_{\mathbf{N}}) &= (\partial_t \xi(t), v_{\mathbf{N}}), \\ (\nabla E_{\mathbf{N}}(t), \nabla \chi_{\mathbf{N}}) - (e_{\mathbf{N}}(t), \chi_{\mathbf{N}}) &= \frac{1}{\varepsilon^2} (f(u(t)) - f(u_{\mathbf{N}}(t)), \chi_{\mathbf{N}}) - (\eta(t), \chi_{\mathbf{N}}), \end{aligned} \quad (2.19)$$

where  $\xi(t) = u(t) - \Pi_{\mathbf{N}}u(t)$  and  $\eta(t) = w(t) - \Pi_{\mathbf{N}}w(t)$ . Taking  $v_{\mathbf{N}} = E_{\mathbf{N}}(t)$ ,  $\chi_{\mathbf{N}} = e_{\mathbf{N}}(t)$  in Eq. (2.19), we obtain

$$\begin{aligned} &\frac{1}{2}\partial_t \|E_{\mathbf{N}}(t)\|_0^2 + \|e_{\mathbf{N}}(t)\|_0^2 \\ &= (\partial_t \xi(t), E_{\mathbf{N}}(t)) + (\eta(t), e_{\mathbf{N}}(t)) + \frac{1}{\varepsilon^2} (f(u_{\mathbf{N}}(t)) - f(u(t)), e_{\mathbf{N}}(t)) \\ &\leq \frac{1}{2}\|\partial_t \xi(t)\|_0^2 + \frac{1}{2}\|E_{\mathbf{N}}(t)\|_0^2 + \|\eta(t)\|_0^2 + \frac{1}{2}\|e_{\mathbf{N}}(t)\|_0^2 + \frac{1}{\varepsilon^4}\|f(u_{\mathbf{N}}(t)) - f(u(t))\|_0^2. \end{aligned}$$

Furthermore, we observe that

$$\|f(u_{\mathbf{N}}(t)) - f(u(t))\|_0 \leq \|u_{\mathbf{N}}(t) - u(t)\|_0 \leq \|\xi(t)\|_0 + \|E_{\mathbf{N}}(t)\|_0.$$

Consequently, for all  $t \in (0, T]$  we have

$$\partial_t \|E_{\mathbf{N}}(t)\|_0^2 + \|e_{\mathbf{N}}(t)\|_0^2 \leq \left(\frac{4}{\varepsilon^4} + 1\right) \|E_{\mathbf{N}}(t)\|_0^2 + \|\partial_t \xi(t)\|_0^2 + \frac{4}{\varepsilon^4} \|\xi(t)\|_0^2 + 2\|\eta(t)\|_0^2,$$

and hence a direct application of the Gronwall inequality gives

$$\|E_{\mathbf{N}}(t)\|_0^2 \lesssim \|E_{\mathbf{N}}(0)\|_0^2 + \int_0^t \left[ \|\partial_\tau \xi(\tau)\|_0^2 + \|\xi(\tau)\|_0^2 + \|\eta(\tau)\|_0^2 \right] d\tau, \quad \forall t \in [0, T].$$

In the same way, we can obtain

$$\int_0^t \|e_{\mathbf{N}}(\tau)\|_0^2 d\tau \lesssim \|E_{\mathbf{N}}(0)\|_0^2 + \int_0^t \left[ \|\partial_\tau \xi(\tau)\|_0^2 + \|\xi(\tau)\|_0^2 + \|\eta(\tau)\|_0^2 \right] d\tau, \quad \forall t \in [0, T].$$

From the triangular inequality and Lemma 2.4,  $\forall t \in [0, T]$  we have

$$\begin{aligned} \|u(t) - u_{\mathbf{N}}(t)\|_0 &\lesssim \|u_{0,\mathbf{N}} - u_0\|_0 + h^{\min(N+1,m)} N^{-m} (\|u(t)\|_m + B(u, w)), \\ \left( \int_0^t \|w(\tau) - w_{\mathbf{N}}(\tau)\|_0^2 d\tau \right)^{\frac{1}{2}} &\lesssim \|u_{0,\mathbf{N}} - u_0\|_0 + h^{\min(N+1,m)} N^{-m} B(u, w), \end{aligned}$$

where

$$B(u, w) = \left( \int_0^T (\|\partial_t u(t)\|_m^2 + \|u(t)\|_m^2 + \|w(t)\|_m^2) dt \right)^{1/2}.$$

Finally, on using Lemma 2.4 once again for  $u_{0,\mathbf{N}}$ , we obtain Eq. (2.18).  $\square$

### 3. Full Discretisation: Splitting Schemes in Time

#### 3.1. A first-order scheme and its error estimate

Let  $M$  be a positive integer,  $\Delta t = T/M$  and consider the following semi-implicit scheme. Find  $(u_{\mathbf{N}}^{n+1}, w_{\mathbf{N}}^{n+1}) \in P_{\mathbf{N}}(\Omega) \times P_{\mathbf{N}}(\Omega)$ ,  $n = 0, 1, \dots, M-1$  such that

$$\left( \frac{u_{\mathbf{N}}^{n+1} - u_{\mathbf{N}}^n}{\Delta t}, v_{\mathbf{N}} \right) + (\nabla w_{\mathbf{N}}^{n+1}, \nabla v_{\mathbf{N}}) = 0, \quad \forall v_{\mathbf{N}} \in P_{\mathbf{N}}(\Omega), \quad (3.1)$$

$$(\nabla u_{\mathbf{N}}^{n+1}, \nabla \chi_{\mathbf{N}}) - (w_{\mathbf{N}}^{n+1}, \chi_{\mathbf{N}}) = -\frac{1}{\varepsilon^2} (f(u_{\mathbf{N}}^n), \chi_{\mathbf{N}}), \quad \forall \chi_{\mathbf{N}} \in P_{\mathbf{N}}(\Omega). \quad (3.2)$$

Formally, this is a first-order scheme, and its stability was proven in Ref. [29] under the condition  $\Delta t \leq 4\varepsilon^4$ . To improve the stability property, we propose to add an extra stability term  $O(\Delta t \partial_t u)$  into Eq. (3.2) with a positive amplitude coefficient  $S$ :

$$(\nabla u_{\mathbf{N}}^{n+1}, \nabla \chi_{\mathbf{N}}) - (w_{\mathbf{N}}^{n+1}, \chi_{\mathbf{N}}) + \frac{S}{\varepsilon^2} (u_{\mathbf{N}}^{n+1} - u_{\mathbf{N}}^n, \chi_{\mathbf{N}}) = -\frac{1}{\varepsilon^2} (f(u_{\mathbf{N}}^n), \chi_{\mathbf{N}}). \quad (3.3)$$

**Lemma 3.1.** *If  $S \geq 1/2$ , then for all  $m \geq 1$  the solution of Eq. (3.3) satisfies*

$$E(u_{\mathbf{N}}^m) + \Delta t \sum_{n=1}^m \|\nabla w_{\mathbf{N}}^n\|_0^2 \leq E(u_0). \quad (3.4)$$

*Proof.* The proof is similar to that for Lemma 3.2 in [29], where the spatial discretisation used a spectral-Galerkin method.  $\square$

This Lemma implies that the energy  $E(u_{\mathbf{N}}^m)$  remains bounded during the computation if  $S$  in Eq. (3.3) is reasonably large.

**Lemma 3.2.**  $(u_{\mathbf{N}}^n, 1) = (u_0, 1)$ ,  $n = 1, 2, \dots, M$ .

*Proof.* For  $v_N = 1$  in Eq. (3.1), we have

$$(u_N^{n+1}, 1) = (u_N^n, 1), \quad n = 1, 2, \dots, M,$$

hence

$$(u_N^n, 1) = (u_N^0, 1) = (\Pi_N u_0, 1) = (u_0, 1), \quad n = 1, 2, \dots, M.$$

□

Similar to Lemma 2.3, we can prove the boundedness of the full discrete solution in the  $H^1$  norm, as stated in the following lemma.

**Lemma 3.3.** *There exists a constant  $c(u_0)$ , depending only on  $u_0$ , such that*

$$\|u_N^n\|_1 \leq c(u_0), \quad n = 0, 1, \dots, M. \tag{3.5}$$

**Theorem 3.1.** *Let  $(u, w)$  be the solution of (2.5)–(2.7), and  $(u_N^n, w_N^n)$  of (3.1)–(3.3). Suppose  $u, w \in L^\infty[(0, T), H^m(\Omega)]$  and  $\partial_t u \in L^\infty[(0, T), H^m(\Omega)] \cap L^2[(0, T), H^m(\Omega)]$ . Then*

$$\|u_N^n - u(t_n)\|_0 \lesssim K_1 h^{\min(N+1, m)} N^{-m} + K_2(1+S)\Delta t, \quad n = 1, 2, \dots, M,$$

where

$$K_1 = \|u\|_{L^\infty[(0, T), H^m(\Omega)]} + \left( \int_0^T \left( \|\partial_t u(t)\|_m^2 + \|w(t)\|_m^2 \right) dt \right)^{\frac{1}{2}},$$

$$K_2 = \left( \int_0^T \left( \|\partial_t u(t)\|_m^2 + \|\partial_t w(t)\|_m^2 \right) dt \right)^{\frac{1}{2}}.$$

We omit the proof of the above estimate, which can be accomplished on the same lines as that in Ref. [29], and it is notable that Theorem 3.1 can be regarded as an extension of the result there. Our extension is twofold: firstly, the present spatial discretisation makes use of a multi-domain spectral element method; and secondly, the effect of the extra stability term on the error is made evident by proving that the extra error decays linearly with the amplitude coefficient  $S$ .

### 3.2. Higher-order schemes

The accuracy in time can be improved by using higher-order semi-implicit schemes, such as described in this subsection.

#### A second-order scheme

By using a second-order backward differentiation for the time derivative term, a second-order extrapolation for the explicit treatment of the nonlinear term, and a second-order stabilisation term, we get the following overall second-order scheme.

Find  $(u_N^{n+1}, w_N^{n+1}) \in P_N(\Omega) \times P_N(\Omega)$ ,  $n = 0, 1, \dots, M - 1$  such that

$$\left( \frac{3u_N^{n+1} - 4u_N^n + u_N^{n-1}}{2\Delta t}, v_N \right) + (\nabla w_N^{n+1}, \nabla v_N) = 0, \quad \forall v_N \in P_N(\Omega), \quad (3.6)$$

$$\begin{aligned} & (\nabla u_N^{n+1}, \nabla \chi_N) - (w_N^{n+1}, \chi_N) + \frac{S}{\varepsilon^2} (u_N^{n+1} - 2u_N^n + u_N^{n-1}, \chi_N) \\ &= -\frac{1}{\varepsilon^2} \left( 2 \left( f(u_N^n) - f(u_N^{n-1}), \chi_N \right) \right), \quad \forall \chi_N \in P_N(\Omega). \end{aligned} \quad (3.7)$$

### A third-order scheme

A third-order scheme can be constructed in a similar way, as follows.

Find  $(u_N^{n+1}, w_N^{n+1}) \in P_N(\Omega) \times P_N(\Omega)$ ,  $n = 0, 1, \dots, M - 1$  such that

$$\left( \frac{11u_N^{n+1} - 18u_N^n + 9u_N^{n-1} - 2u_N^{n-2}}{6\Delta t}, v_N \right) + (\nabla w_N^{n+1}, \nabla v_N) = 0, \quad \forall v_N \in P_N(\Omega), \quad (3.8)$$

$$\begin{aligned} & (\nabla u_N^{n+1}, \nabla \chi_N) - (w_N^{n+1}, \chi_N) + \frac{S}{\varepsilon^2} (u_N^{n+1} - 3u_N^n + 3u_N^{n-1} - u_N^{n-2}, \chi_N) \\ &= -\frac{1}{\varepsilon^2} \left( (3f(u_N^n) - 3f(u_N^{n-1}) + f(u_N^{n-2}), \chi_N) \right), \quad \forall \chi_N \in P_N(\Omega). \end{aligned} \quad (3.9)$$

A detailed analysis of these schemes is beyond the scope of the current work and remains an important next step for future research. However, a numerical comparison for the schemes constructed above is undertaken in the next section.

## 4. Numerical Results and Discussion

We first carry out a numerical test to validate the error estimate. Consider the Cahn-Hilliard equation

$$\partial_t u + \Delta(u - u^3 + \gamma \Delta u) = f, \quad (\mathbf{x}, t) \in \Omega \times (0, 1), \quad (4.1)$$

with the analytical solution

$$u(x, y, t) = e^{\cos(t)} \cos(\pi x) \cos(\pi y), \quad (x, y) \in \Omega = [-1, 1] \times [-1, 1], \quad 0 < t < 1.$$

In Eq. (4.1),  $f$  is computed from the left-hand side by using the exact solution and  $\gamma = 0.1$ , and  $u_0$  is taken to be consistent with the exact solution.

The left figure in Fig. 1 shows the  $L^2$ -norm errors as a function of the time step size for two values of  $S$ , using the first-order scheme. We observe that the error curves are all straight lines of slope 1 in a logarithmic-logarithmic scale plot, which indicates that the errors decay linearly as  $\Delta t$  decreases. The  $L^2$ -norm errors versus the parameter  $S$  are presented in the right figure of Fig. 1, which clearly shows the linear dependence of the errors on  $S$  as predicted by Theorem 3.1. The error behaviour with respect to the spatial discretisation parameters is presented in Fig. 2. In the left figure, the errors in

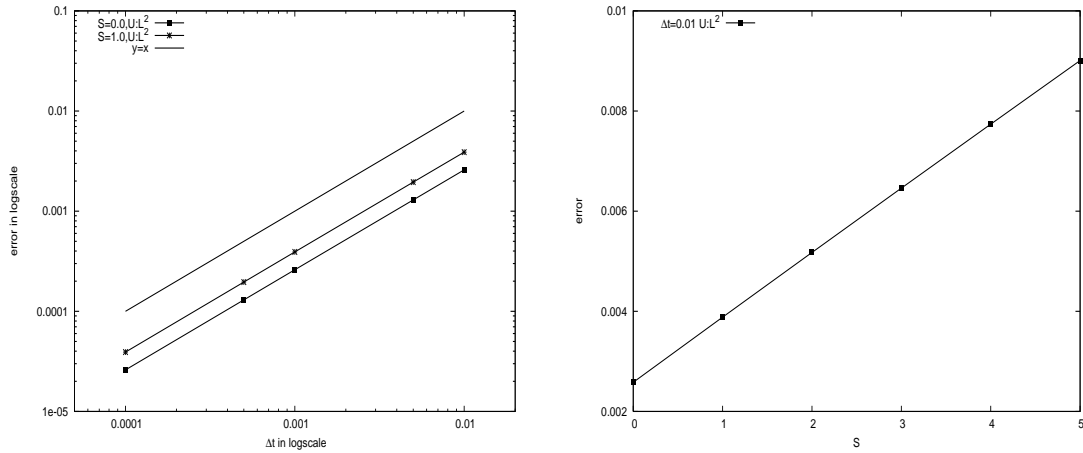


Figure 1: Errors at  $t = 1$  in the  $L^2$ -norm as a function of  $\Delta t$  (left) and  $S$  (right), using the first-order scheme with  $K = 1$  and  $N = 24$ .

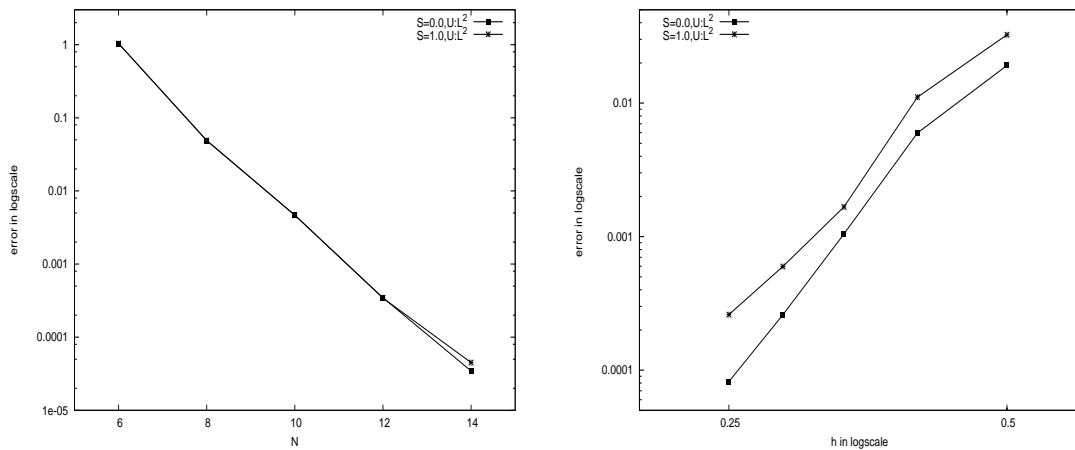


Figure 2: Errors at  $t = 1$  in the  $L^2$ -norm as a function of  $N$  (left) and  $h$  (right), using the first-order scheme with  $\Delta t = 0.0001$ ,  $K = 1$  (left) and  $N = 3$  (right).

semi-logarithmic scale are shown versus the polynomial degree  $N$ , and the straight lines are evidence of the exponential convergence in space of the numerical solutions. The right figure in Fig. 2 plots the  $L^2$ -norm errors as functions of the spectral element size  $h$  in logarithmic-logarithmic scale, corresponding to an algebraic convergence rate.

We repeat the same test for higher-order schemes. In Fig. 3, we plot the error history for the second-order scheme (3.6)–(3.7) as functions of the time step size  $\Delta t$  (left figure) and stabilisation parameter  $S$  (right figure), respectively. Clearly, the error curves are straight lines of slope 2 in the left figure, indicating there is second-order convergence in time. Furthermore, in the right figure we see that there is again linear dependence of the error on  $S$  for the second-order scheme. The spatial discretisation errors with respect to the discretisation parameters  $N$  and  $h$  are shown in Fig. 4. As expected, the convergence

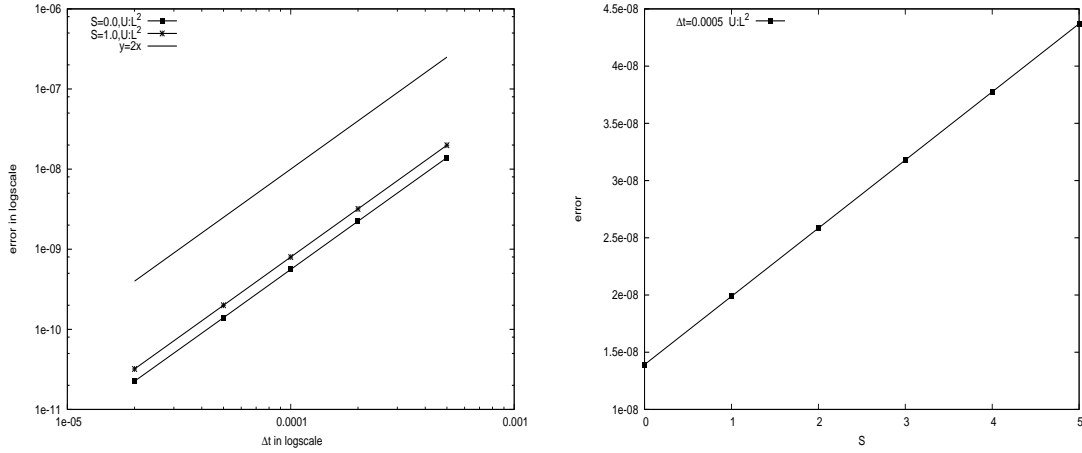


Figure 3: Errors at  $T = 1$  versus  $\Delta t$  (left) and  $S$  (right) computed by using the second-order scheme (3.6)–(3.7) with  $K = 1$ ,  $N = 24$ .

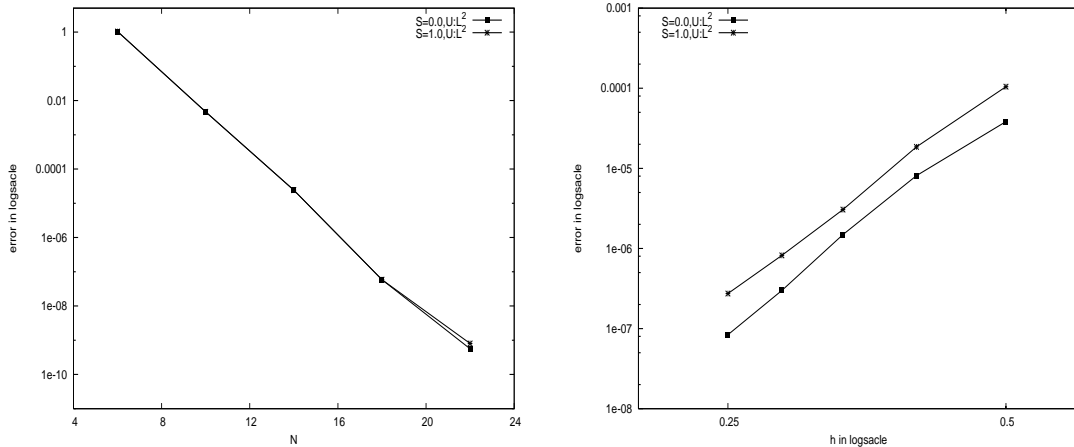


Figure 4:  $L^2$ -errors as a function of  $N$  (left) and  $h$  (right) using the second-order scheme (3.6)–(3.7) with  $\Delta t = 0.0001$ ,  $K = 1$  (left), and  $N = 5$  (right).

is exponential in  $N$  and algebraic with respect to  $h$ .

In order to investigate the convergence property of the third-order scheme numerically, we use (3.8)–(3.9) to compute the solution with the fixed spectral element parameters  $K = 1$  and  $N = 32$ . The result presented in Fig. 5 shows the error decay rate with respect to  $\Delta t$  in the left figure, and the decay rate with respect to  $S$  in the right figure. Although not yet proven rigorously, this demonstrates that the error behaviour induced by the time discretisation (3.8)–(3.9) is  $O((S + 1)\Delta t^3)$ .

We now consider a system modelling a specific type of mixture of two incompressible

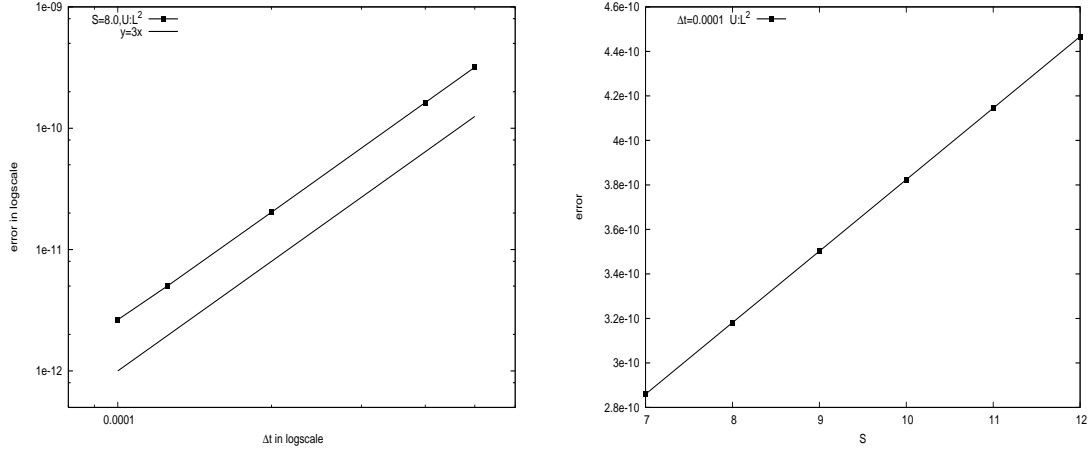


Figure 5: Error decay with respect to  $\Delta t$  (left) and  $S$  (right) using the scheme (3.8)–(3.9) with  $K = 1$  and  $N = 32$ .

fluids with variable density and viscosity in  $Q_T =: \Omega \times (0, T)$ :

$$\begin{cases} \partial_t(\rho(\phi)\mathbf{u}) + \mathbf{u} \cdot \nabla(\rho(\phi)\mathbf{u}) + \nabla p - \nabla \cdot (\nu(\phi)D(\mathbf{u})) + \lambda \nabla \cdot (\nabla \phi \otimes \nabla \phi) = \mathbf{g}, \\ \nabla \cdot \mathbf{u} = 0, \\ \partial_t \phi + \mathbf{u} \cdot \nabla \phi = -\gamma \Delta \left( \Delta \phi - \frac{1}{\varepsilon^2} f(\phi) \right), \end{cases}$$

subject to the initial conditions

$$\mathbf{u}(\mathbf{x}, 0) = \mathbf{u}_0(\mathbf{x}), \quad \phi(\mathbf{x}, 0) = \phi_0(\mathbf{x}), \quad \mathbf{x} \in \Omega,$$

and the boundary conditions

$$\mathbf{u} = \mathbf{0}, \quad \frac{\partial \phi}{\partial \mathbf{n}} = \frac{\partial^3 \phi}{\partial \mathbf{n}^3} = \mathbf{0}, \quad \text{on } \partial \Omega \times (0, T). \quad (4.2)$$

Here the density  $\rho$  satisfies the continuity equation

$$\partial_t \rho + \nabla \cdot (\rho \mathbf{u}) = 0,$$

$\mathbf{u}$  represents the velocity vector of the fluids,  $p$  is the pressure,  $\phi$  represents the “phase” of the molecules,  $\nu$  is the viscosity coefficient,  $D(\mathbf{u}) = (\nabla \mathbf{u} + (\nabla \mathbf{u})^T)/2$  is the stretching tensor,  $\lambda$  corresponds to the surface tension,  $\mathbf{g}$  is the external body force,  $\gamma$  represents the elastic relaxation time of the system, and  $f(\phi) = F'(\phi)$  with  $F(\phi) = (\phi^2 - 1)^2/4$  standing for the bulk part of the mixing energy.

However, for our calculations we use the following simplified model equation [23]:

$$\begin{aligned} & \bar{\rho} (\partial_t \mathbf{u} + \mathbf{u} \cdot \nabla \mathbf{u}) + \nabla p - \nabla \cdot (\nu D(\mathbf{u})) + \lambda \nabla \cdot (\nabla \phi \otimes \nabla \phi) \\ & = -(1 + \phi)(\rho_1 - \bar{\rho})\mathbf{g} - (1 - \phi)(\rho_2 - \bar{\rho})\mathbf{g}, \end{aligned}$$

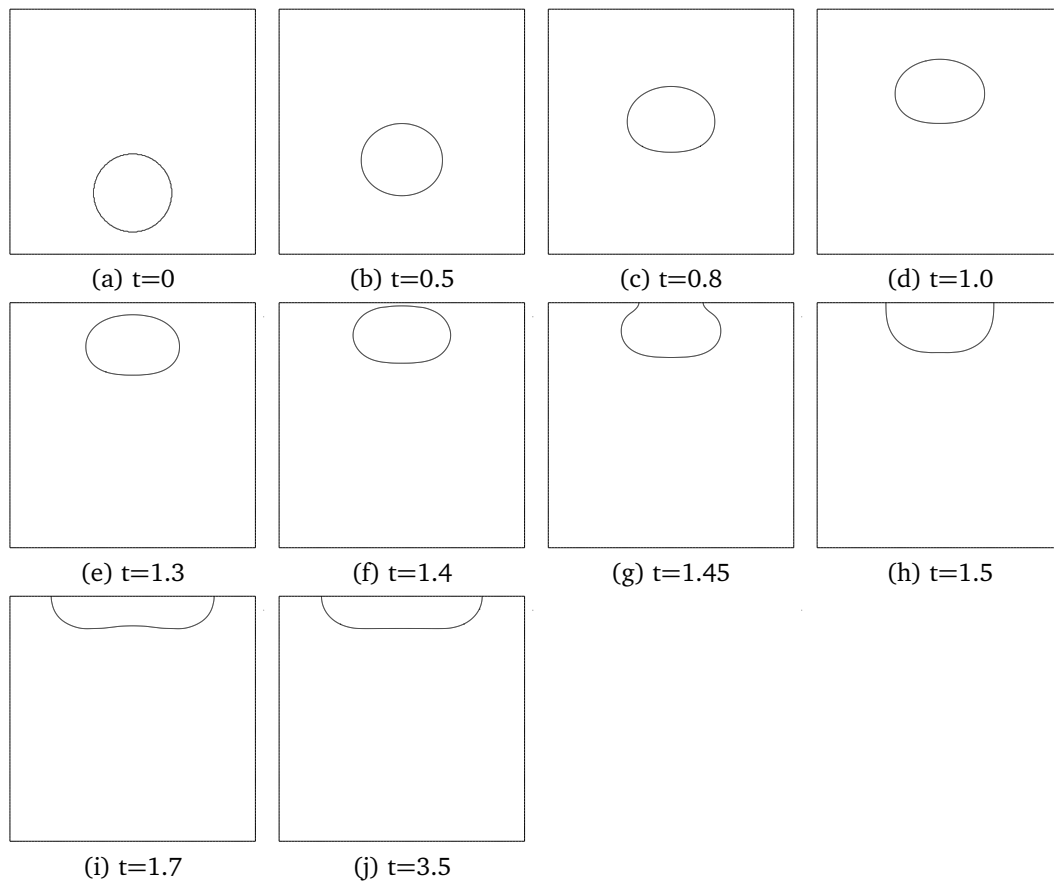
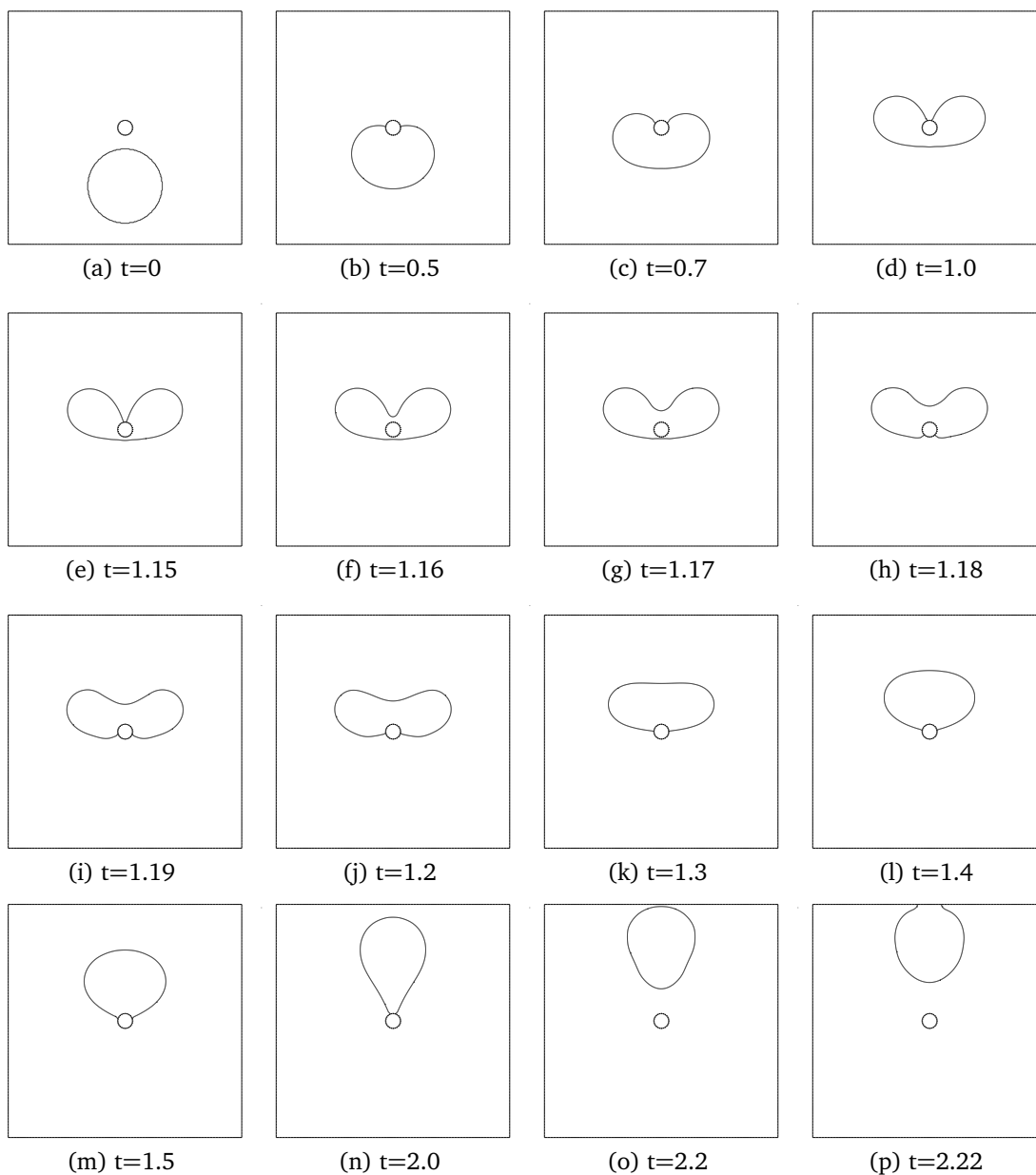


Figure 6: Phase evolution at different times, for the computed domain  $[0, 2\pi] \times [0, 2\pi]$  decomposed into 6400 elements.

where  $\bar{\rho} = (\rho_1 + \rho_2)/2$  and  $\mathbf{g}$  is the gravitational acceleration. In all cases, we have used the second-order scheme and spectral element method for the respective time and space discretisations of the model, with the computational parameters  $N = 5$  and  $\Delta t = 0.0005$  and the following physical parameters:

$$\begin{aligned} \varepsilon &= 0.02, \quad \lambda = 0.1, \quad \nu = 0.1, \quad \gamma = 0.1, \quad S = 2, \\ \rho_1 &= 0.5, \quad \rho_2 = 1.5, \quad \mathbf{g} = (0, -10)^T, \\ \mathbf{u}_0(\mathbf{x}) &= \mathbf{0}, \quad \forall \mathbf{x} \in \Omega, \\ \phi_0(\mathbf{x}) &= \begin{cases} 1 & \text{for } \mathbf{x} \text{ inside the bubble,} \\ -1 & \text{for } \mathbf{x} \text{ outside the bubble.} \end{cases} \end{aligned}$$

**Test 1** The simulation starts with a circular bubble near the bottom of the domain. The density of the bubble is less than the density of the surrounding flow. The computational domain is  $[0, 2\pi] \times [0, 2\pi]$ , broken into 6400 equal elements. Fig. 6 shows the evolution history of the bubble, which rises progressively due to buoyancy until the bubble touches



cont'd ...

the top side. This result is in a good agreement with previously published work — e.g. see Ref. [23].

**Test 2** Consider a bubble rising in a domain containing a small obstacle at the centre. The phase field equations are solved in the domain  $[0, 2\pi] \times [0, 2\pi] \setminus \{(x, y) | (x - \pi)^2 + (y - \pi)^2 \leq 0.2^2\}$ , with the spectral element mesh consisting of 6388 macro elements of

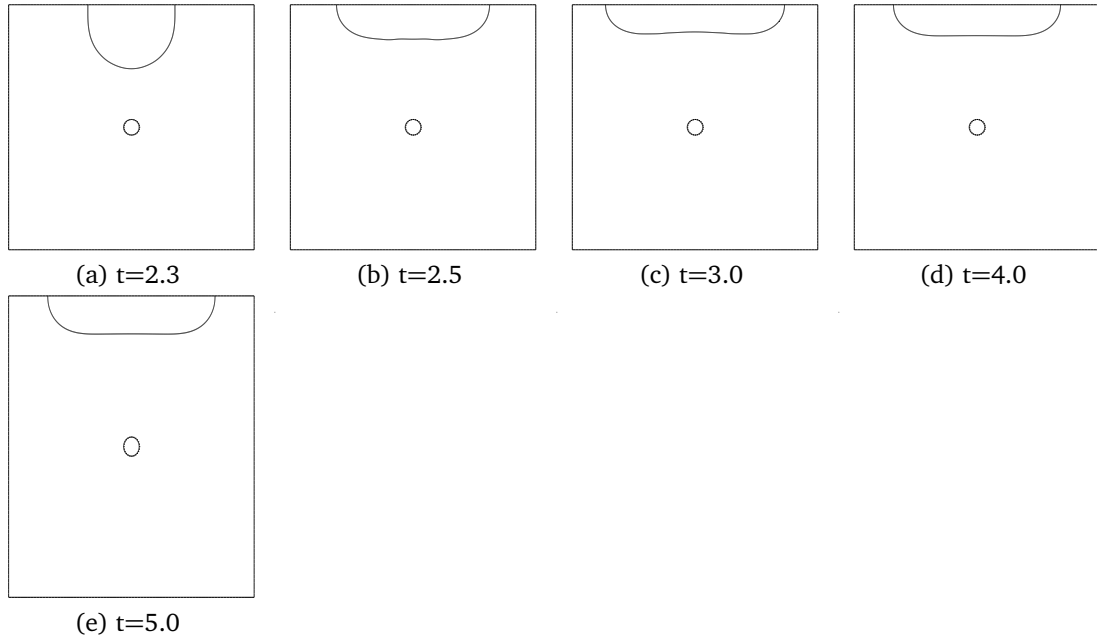


Figure 7: Phase evolution at different times, for the computed domain  $[0, 2\pi] \times [0, 2\pi] \setminus \{(x, y) | (x - \pi)^2 + (y - \pi)^2 \leq 0.2^2\}$  decomposed into 6388 elements.

polynomial degree  $N = 5$  in each element. The circular bubble is initially placed close to the bottom edge. Fig. 7 illustrates the bubble rising during the time evolution, where we observe that the bubble continues to rise after it touches the obstacle, which envelops the entire bubble during some time period before the obstacle is reached. Finally, the bubble stops moving at some time after touching the top edge of the domain. Incidentally, the bubble remains connected during the whole time evolution.

**Test 3** In this test, the computational configuration is similar to Test 2, but with a bigger obstacle at the centre of the domain — i.e.  $\Omega = [0, 2\pi] \times [0, 2\pi] \setminus \{(x, y) | (x - \pi)^2 + (y - \pi)^2 \leq 0.5^2\}$ . This simulation uses 6260 macro spectral elements. We repeated the calculation as in Test 2, and Fig. 8 again shows some snapshots of the rising bubble at different time instants. As it crosses the obstacle, the bubble first breaks into two separate bubbles but then reassembles again into one complete unit. Another feature is that its rise slows down compared to the evolution in Test 2, suggesting that the bigger the obstacle size the slower the rising speed of the bubble. To the best of our knowledge, this phenomenon has never been reported in the literature, and requires a physical interpretation.

## 5. Conclusion

We have proposed and analysed a class of fully discrete schemes for the Cahn-Hilliard equation with Neumann boundary conditions. The proposed schemes combine time split-

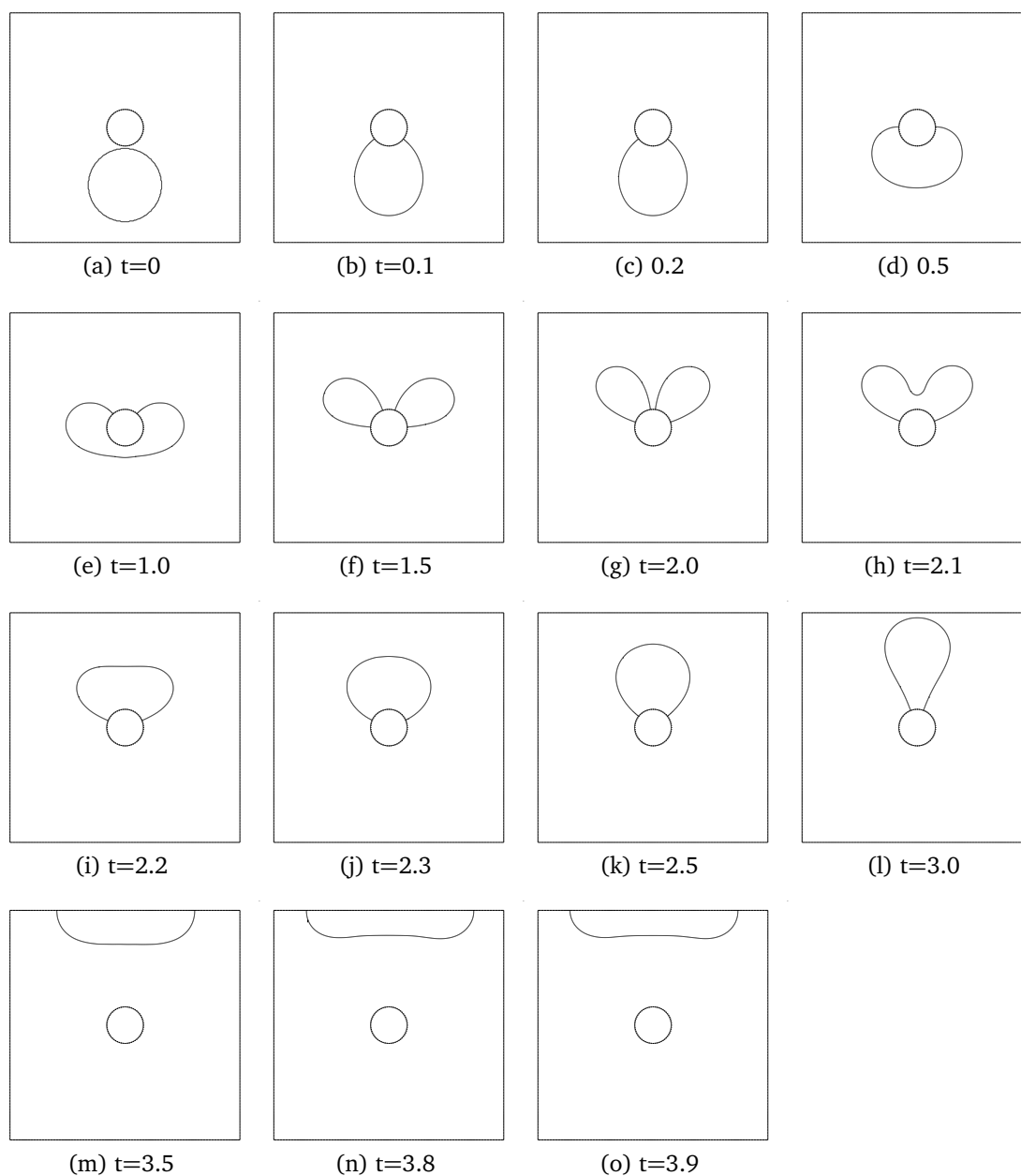


Figure 8: Bubble rising snapshots at various time instants in the domain  $[0, 2\pi] \times [0, 2\pi] \setminus \{(x, y) | (x - \pi)^2 + (y - \pi)^2 \leq 0.5^2\}$ , using a spectral element mesh with 6260 macro elements.

ting methods and spatial spectral element methods, allowing us to take advantage of both time and space schemes. Stability and convergence properties were established for the first-order time scheme. The higher-order schemes were not analysed, but investigated

through a number of numerical examples. The proposed schemes were applied to a phase field simulation in complex geometry, and some new interesting phenomena have been observed. Although the present work only addresses Neumann boundary conditions, the results obtained remain valid for the Dirichlet conditions  $u = \partial^2 u / \partial \mathbf{n}^2 = 0$  on  $\partial \Omega$  when the solution space  $H^1(\Omega)$  is replaced with  $H_0^1(\Omega)$ .

### Acknowledgments

The research of first author was supported by NSF of China under Grant 11301438. The research of second author was partially supported by NSF of China (Grant numbers 11071203 and 91130002).

### References

- [1] S. Allen and J. W. Cahn, *A microscopic theory for antiphase boundary motion and its application to antiphase domain coarsening*, Acta Metall. **27**, 1084–1095 (1979).
- [2] D. Gottlieb, B. Costa, W. S. Don and R. Sendersky, *Two-dimensional multi-domain hybrid spectral-WENO methods for conservation laws*, Comm. Comput. Phys. **1**, 550–577 (2006).
- [3] J. W. Cahn and J. E. Hilliard, *Free energy of a nonuniform system I. Interfacial free energy*, J. Chem. Phys. **28**, 258–267 (1958).
- [4] L. Q. Chen, *Phase-field models for microstructure evolution*, Annu. Rev. Mater. Res. **32**, 113–140 (2002).
- [5] L. Q. Chen and J. Shen, *Applications of semi-implicit Fourier-spectral method to phase-field equations*, Comput. Phys. Commun. **108**, 147–158 (1998).
- [6] S. M. Choo and S. K. Chung, *Conservative nonlinear difference scheme for the Cahn-Hilliard equation*, Comput. Math. Appl. **36**, 31–39 (1998).
- [7] D. A. French, C. M. Elliott and F. A. Milner, *A second order splitting method for the Cahn-Hilliard equation*, Numerische Mathematik **54**, 575–590 (1989).
- [8] M. I. M. Copetti and C. M. Elliott, *Numerical analysis of the Cahn-Hilliard equation with a logarithmic free energy*, Numer. Math. **63**, 39–65 (1992).
- [9] G. B. McFadden, D. M. Anderson and A. A. Wheeler, *Diffuse-interface methods in fluid mechanics*, Annu. Rev. Fluid Mech. **30**, 139–165 (1998).
- [10] P. de Mottoni and M. Schatzman, *Evolution géométrique d'interfaces*, C. R. Acad. Sci. Paris, Série I, Math. **309**, 453–458 (1989).
- [11] P. de Mottoni and M. Schatzman, *Geometrical evolution of developed interfaces*, Trans. Amer. Math. Soc. **347**, 1533–1589 (1995).
- [12] Q. Du and R. A. Nicolaides, *Numerical analysis of a continuum model of phase transition*, SIAM J. Numer. Anal. **28**, 1310–1322 (1991).
- [13] C. M. Elliott and D. A. French, *Numerical studies of the Cahn-Hilliard equation for phase separation*, IMA J. Appl. Math **38**, 97–128 (1987).
- [14] C. M. Elliott and D. A. French, *A nonconforming finite-element method for the two-dimensional Cahn-Hilliard equation*, SIAM J. Numer. Anal. **26**, 884–903 (1989).
- [15] C. M. Elliott and S. Larsson, *Error estimates with smooth and nonsmooth data for a finite element method for the Cahn-Hilliard equation*, Math. Comput. **58**, 603–630 (1992).
- [16] C. M. Elliott and Z. Songmu, *On the Cahn-Hilliard equation*, Arch. Ration. Mech. An. **96**, 339–357 (1986).

- [17] D. Furihata, *A stable and conservative finite difference scheme for the Cahn-Hilliard equation*, Numerische Mathematik **87**, 675–699 (2001).
- [18] L. P. He, *Error estimation of a class of stable spectral approximation to the Cahn-Hilliard equation*, J. Sci. Comput. **41**, 461–482 (2009).
- [19] T. Ilmanen, *Convergence of the Allen-Cahn equation to Brakkeq’s motion by mean curvature*, J. Differential Geom. **38**, 417–461 (1993).
- [20] J. F. Blowey, J. W. Barrett and H. Garcke, *On fully practical finite element approximations of degenerate Cahn-Hilliard systems*, Math. Model. Numer. Anal. **35**, 713–748 (2001).
- [21] J. Kim, *Phase-field models for multi-component fluid flows*, Commun. Comput. Phys. **12**, 613–661 (2012).
- [22] H. M. Soner, L. C. Evans and P. E. Souganidis, *Phase transitions and generalized motion by mean curvature*, Comm. Pure Appl. Math. **45**, 1097–1123 (1992).
- [23] C. Liu and J. Shen, *A phase field model for the mixture of two incompressible fluids and its approximation by a Fourier-spectral method*, Physica D: Nonlinear Phenomena **179**, 211–228 (2003).
- [24] C. Liu and N. J. Walkington, *An Eulerian description of fluids containing visco-elastic particles*, Arch. Rational Mesh. Anal. **159**, 229–252 (2001).
- [25] J. Lowengrub and L. Truskinovsky, *Quasi-incompressible Cahn-Hilliard fluids and topological transitions*, Proc. R. Soc. Lond. A **454**, 2617–2654 (1998).
- [26] C. Liu, P. Yue, J. J. Feng and J. Shen, *A diffuse-interface method for simulating two-phase flows of complex fluids*, J. Fluid Mech. **515**, 293–317 (2004).
- [27] B. Guo, Q. Du and J. Shen, *Fourier spectral approximation to a dissipative system modeling the flow of liquid crystals*, SIAM J. Numer. Anal. **39**, 735–762 (2002).
- [28] C. Liu, Q. Du and X. Wang, *Simulating the deformation of vesicle membranes under elastic bending energy in three dimensions*, J. Comput. Phys. **212**, 757–777 (2005).
- [29] J. Shen and X. F. Yang, *Numerical approximations of Allen-Cahn and Cahn-Hilliard equations*, DCDS-A **28**, 1669–1691 (2010).
- [30] X. Feng, T. Tang, and J. Yang, *Stabilized Crank-Nicolson/Adams-Bashforth schemes for phase field models*, East Asian J. Appl. Math. **3**, 59–80 (2013).
- [31] C. Liu, X. Yang, J. J. Feng and J. Shen, *Numerical simulations of jet pinching-off and drop formation using an energetic variational phase-field method*, J. Comput. Phys. **218**, 417–428 (2006).
- [32] X. Ye and X. Cheng, *Legendre spectral approximation for the Cahn-Hilliard equation*, Mathematica Numerica Sinica **2**, 157-170 (2003).
- [33] Y. Liu, Y. He and T. Tang, *On large time-stepping methods for the Cahn-Hilliard equation*, Appl. Numer. Math. **57**, 616–628 (2007).
- [34] Q. Q. Zhuang and C. J. Xu, *A spectral element/Laguerre coupled method to the elliptic Helmholtz problem on the half line*, Numerical Mathematics A, Journal of Chinese Universities English Series **15**, 193–208 (2006).